Compressive Sensing Techniques for Radar and ESM Applications:
Part II: Hardware Architectures for Compressive Sensing

Emre Ertin
Department of Electrical and Computer Engineering
The Ohio State University
Columbus, Ohio

Distribution A. Approved for Public Release: distribution unlimited
(Approval given by the 88th ABW PA Approval Office under case number 88ABW-2019-0638)

2.0 Hardware Architectures for Compressive Sensing

2.1 Introduction

Radar systems acquire information about the scene of interest by transmitting pulsed waveforms and analyzing the received backscatter energy to form an estimate of the distance, direction and velocity information of the reflectors in the scene. Range resolution of a radar sensor is defined as the minimum separation between two reflectors on the same bearing but at different ranges that the system can detect as distinct points. Range resolution is inversely proportional to the bandwidth of the radar system [1].

In order to improve range resolution and consequently to detect closely spaced targets, modern day radars typically operate with bandwidths approaching to Gigahertz. Receiver processing starts by forming an estimate of the range profile through a match filtering process where the received backscatter energy is correlated with a copy of the transmitted signal. To implement match filtering processing in a digital system using Analog to Digital Converters (ADC), the receiver must sample the signal at *Nyquist rate*, which is at least twice the bandwidth of the system for the duration of the pulse. However, commercially available ADCs do not meet the requirements of next generation radar systems with exceedingly large bandwidths. Operating ADCs at sampling rates beyond rates of GSamples per second results in tradeoff in the form of reduced dynamic range [2] of 5-8 bits. In addition, the power consumption of thermal limited ADCs quadruples with every additional bit [2]. Power considerations restricts deployment of wide bandwidth radars on mobile platforms with limited size and power budgets for the sensor payload. Therefore for high resolution radar systems, dynamic range and power constraints on commercially available ADCs will continue to be a bottleneck, imposing a practical lower bound on the maximum achievable range resolution for digital systems.

This problem is further exacerbated by the need for high spatial resolution in Multi Input Multi Output (MIMO) radar systems. As higher spatial is only possible with increasing the size of the aperture or the effective length of the antenna array. As a result high speed DAC/ADCs have to be employed at each transmit/receive channel and the digital backend has to be designed to handle the large volume of samples generated in digitization of the received energy, both adding to the overall cost and complexity of the system rendering large scale digital MIMO radar systems impractical with the current commercially available devices.

An alternate approach to this problem is using *Stretch processing* [3, 4] on the receiver which converts a range estimation problem into a frequency estimation problem. In the specific case of a linear frequency modulated waveform (LFM) $\phi(t) = e^{j\beta t^2}$ used on transmit, the matched filtering can be approximately implemented through mixing the received signal with a reference LFM waveform and low pass filtering the mixer output [1]. At the receiver output, the transmitted waveform delayed by Δ appears as a sinusoidal tone whose frequency is given by $\beta\Delta$ as illustrated in Figure 1. The Nyquist sampling rate of the ADC is proportional the bandwidth of LFM chirp scaled down by the $\frac{T_u}{\tau}$ ratio, where T_u and τ are time spread of the reflectors in the scene (unambiguous range) and pulse length respectively. Even though this dechirped signal has lower bandwidth than the original transmit signal, the resulting Nyquist rate can be still constraining factor for the receiver design if the unambiguous range is large.

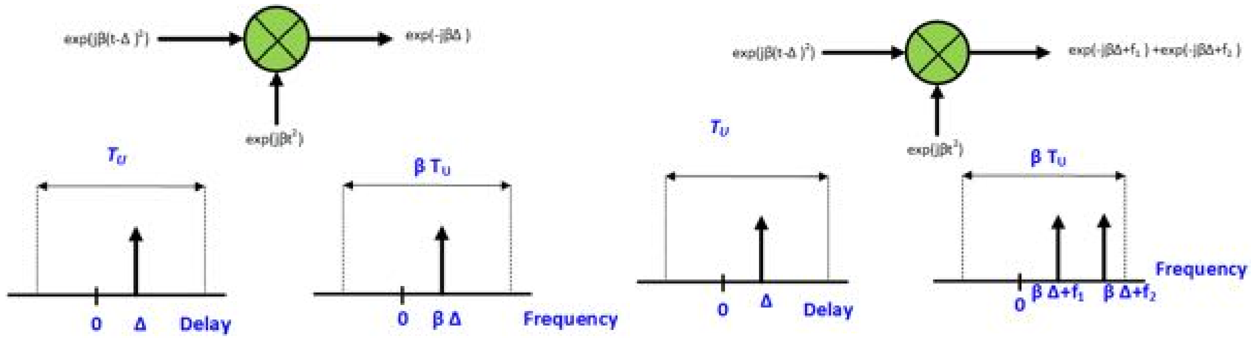

(a) Single target with one tone

(b) Single target with two tones

Figure 1: Effect of stretch processing

2.2 Receiver-side Hardware Architectures for Compressive Sensing

Over the past several years, compressive sensing (CS) has emerged as a new framework for signal acquisition at sub-Nyquist sampling rates through randomized linear projections with provable performance guarantees for recovery of structured signals. CS framework was adapted to radar domain [5] in various application contexts: range profile estimation [6], waveform design using frequency hopping codes for estimation in range, Doppler velocity and angle domain [7], waveform design using a multi-objective optimization of a combination of mutual coherence and signal to interference ratio [8], single pulse systems for range and Doppler velocity estimation [9], single pulse multiple transmit and receive system for range, Doppler-velocity and azimuth estimation and target detection [10, 11, 12], remote sensing [13] and estimation of range, angle of arrival and Doppler velocity using stepped frequency multi-pulse MIMO radar employing stochastic waveform in each transmitter [14, 15].

Although theoretical foundations for compressive sensing and sub-Nyquist sampling is well established in the past decade, relatively few hardware implementations of these theoretical concepts emerged in the radar domain. Shastry *et al* describes a compressively sampled noise radar system for Ultrawideband (UWB) radar imaging and [16] shows the practical implementation of the compressively sampled noise radar for automotive application. Unlike a pulse radar system, continuous-wave noise radar system is simple to design and implement owing to the lack of synchronization requirement. However, digital generation of wide bandwidth noise source at the transmitter requires a huge amount of samples which puts a constraint on the memory. The other options being using analog noise generators which are readily available in the market. However, when using an analog noise source for generating transmit waveform, a dedicated ADC channel has to be assigned to the receiver for sampling the transmit noise for match filtering purpose. Moreover, the Peak to Power Ratio (PAPR) of the noise waveforms is theoretically infinity which leads to nonlinearity issues while using power amplifiers on transmit side to achieve range.

T.Ragheb *et al* describes a prototype hardware implementation of a random demodulation based compressive ADC (CADC) which can be used in radars for sub-Nyquist sampling of received signal in [17]. Figure 2 shows the hardware block diagram of CADC prototype. In this method, the input signal is modulated by a square pulse, with pseudo-random values of ± 1, generated by a Pseudo Noise (PN) sequence. This process spreads the frequency content over a wider bandwidth to preserve its information content for the second stage. This signal is low pass filtered and sampled by a traditional ADC. The dynamic range of the proposed

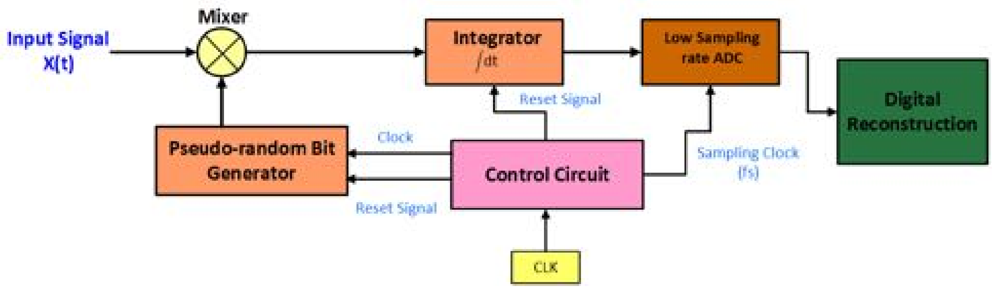

Figure 2: Hardware block diagram of CADC prototype as described in [17]

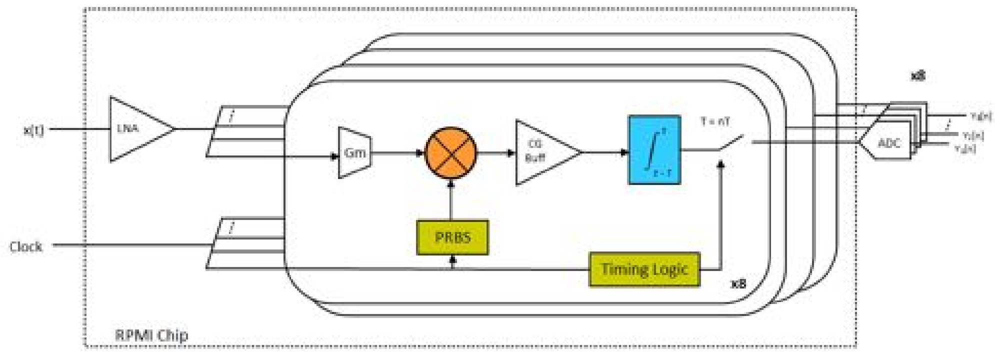

Figure 3: Simplified block diagram of RMPI as described in [19]

compressive ADC is limited by clock jitter of the random number generator, the linearity and intermodulation distortion of the mixer, and the quantization error of the backend ADC [18, 19]. Moreover, the pseudo random binary sequence needed for modulating the input signal needs to be generated at the Nyquist rate of the input signal which puts a practical constraint on the maximum achievable bandwidth of the system. J. Yoo *et al* describes a Complimentary Metal Oxide Semiconductor (CMOS) implementation of a Compressive ADC based receiver which has an analog bandwidth of 100 MHz - 2 GHz with a dynamic range of about 54 dB in [19]. A simplified bloack diagram of the proposed system is shown in 3. The proposed ADC samples the 1.9 GHz bandwidth signal at 320MSPS - a factor 12.5x lower than the Nyquist rate. However, implementation of the proposed non-uniform sampling system requires the entire ADC to be redesigned for this specific application, which in turn adds to the cost and complexity of the receiver.

Michael *et al* describes a hardware implementation of a wideband, compressed sensing based *non-uniform sampling (NUS)* receiver with custom sample-and-hold circuit design for sub-Nyquist sampling of input signal [20]. Figure 4 shows the simplified block diagram of the NUS receiver. The non-uniformly spaced pulse train generated at Nyquist rate by the timing generator (TG) controls the master and slave sample-and-hold circuit which samples the sparse input signal. The samples from the slave sample-and-hold circuit (SSH) are buffered, amplified and digitized by a non-uniform sampling ADC at a sampling rate much lower than the Nyquist sampling rate of the input signal. Even though this architecture is simple to implement compared to the Compressive ADC architecture [17], input signal needs to follow two important constraints for successful reconstruction of the samples. The first is effective instantaneous bandwidth (EIBW) of the input signal should be less than half the Nyquist rate, and the second is the input signal should have spectral sparsity in order to achieve accurate reconstruction.

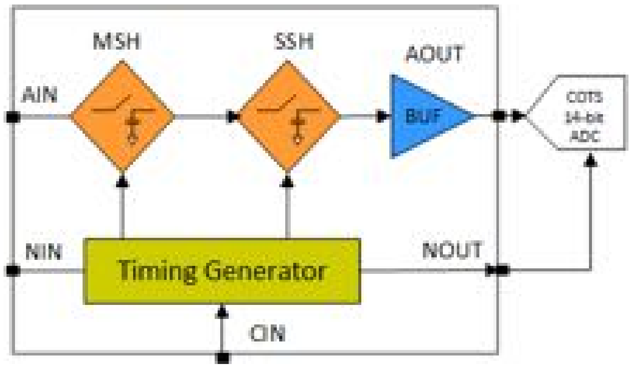

Figure 4: Simplified block diagram of non-uniform sampler (NUS) receiver as described in [20]

Eldar *et al* proposes an alternate compressive sampling architecture which addresses some of the practical limitations of implementation the compressive ADC architecture in [21, 22, 23]. In this approach, the wideband input signal is mixed with highly transient periodic waveform generated using commercial Shift Registers (SR) instead of pseudo-random values of ± 1. This eliminated the need for using expensive Field Programmable Gate Array (FPGA) based PN clock generators or Digital to Analog Converter (DAC) for generating the mixing signal at the Nyquist rate. Moreover, with this modification, a standard switching mixer with equalizer for power control can be used. However, this architecture is bounded by the condition $mf_s \simeq 2NB$. Which means the total sampling rate of the system should be proportional to the bandwidth of each channel and the number of signal bands present in the wideband spectrum. Hence, in practical implementation to recover information from multiple bands while maintaining a low sampling rate, multiple parallel signal paths are used on the receiver which increases the cost and hardware complexity. In addition to this, Eldar *et al* work limits itself to a rapid interference detector and does not address the problem of general purpose reception which are both important for cognitive radio. To address some of the limitations of [21], Doughlas *et al* presents an advanced Modulated Wideband Converter (MWC) architecture for cognitive radio systems that can operate over a wide range of frequencies, dynamically adjust its channel bandwidth, and aggregate multiple signal bands [24]. The proposed system uses delay-based and sequence-based harmonic rejection technique for removing in-band blocker signal which was a limitation of MWC architecture discussed in [21, 22, 23].

A simplified implementation of an analog to digital conversion scheme and a recovery algorithm with relaxed constraints based on Xampling framework [25] has been presented in [26, 27, 28]. The proposed receiver architecture consists of four channels, each comprising of crystal bandpass filter with random effective carrier frequency. The input signal is generated at base band with several random groups of Fourier coefficients. This signal is up-converted to the pass band of the crystal band pass filtered using four discrete Local Oscillator (LO) signals. The band pass filtered signal is again demodulated by a fixed LO and filtered by a low pass filter and sampled at 125 kHz. This results in many fold reduction in sampling rate compared to a traditional receiver. The proposed receiver required three filtering stages and two mixing stages to process the transmitted signal. While using multiple filtering stages adds to the cost of the system, multiple receiver stages suffer from well-known problems like inter-modulations and LO leakages which might degrade the dynamic range of the receiver.

2.3 Transmitter side Hardware Architectures for Compressive Radar

The previous work was based on modifying the receivers to achieve low rate samples that result in appropriate incoherency in the resulting sensing matrix. The receiver side CS architectures are originally proposed for communication systems and can be adopted to radar as well. However, radar system design provides an additional degree of freedom for design, namely the transmitted waveforms. The transmitted waveforms can be tailored to minimize the coherency of the resulting sensing matrix to achieve high resolution in range and angle spae simultaneously.

In the following we will study in detail the estimation problem of range and angle of arrival of targets using a specific MIMO radar architecture employing compressive illumination transmit waveforms that implments randomization in the transmit signal structure while minimizing receiver design complexity through a simple stretch processor. This compressive illumination approach is based on the observation that LFM waveforms and analog stretch processing converts the range estimation problem into an equivalent sparse frequency spectrum estimation problem. The proposed scheme can be readily implemented utilizing a small number of random parameters in waveform generation (frequency and phase) and low speed uniform sampling ADCs with high analog bandwidth at the receiver. ADCs whose analog bandwidth exceed their maximum sampling rate by several factors are readily available commercially and used routinely in pass-band sampling. This compressive radar structure termed as compressive illumination was first proposed in [29, 30] and uses a linear combination of sinusoids to modulate an LFM waveform at the transmitter with randomly selected center frequencies, while maintaining the simple standard stretch processing receiver structure. The output of the stretch processor receiver is given by $y(t) = \sum_{n=1}^{N} x_n \sum_{k=1}^{N_c} e^{(j\phi_{n,k})} e^{(j(n\beta\Delta+\omega_k)t)}$ where $\phi_{n,k}$ is a predetermined known complex phase, N_c is the number of tones modulating the LFM waveform. We observe that under the proposed compressive sensor design each delayed copy of the transmitted waveform is mapped to multi-tone spectra with known structure.

2.4 A prototype implementation of Compressive Illumination

2.4.1 System Architecture

This proposed radar testbed is made up of a custom-built RF Frontend featuring 16 S-band (3100 MHz) transmit channels and one receive channel along with a digital backend comprising of a Nutaq Picodigitizers and four Analog Devices Direct Digital Synthesizers (DDS) boards. The block diagram of the proposed system is shown in Figure 5. The multitone waveform is generated using AD9959 DDS board. Each chip contains four DDS core within them, so a total of four DDS modules are used to generate 16 tones which serve as IF signals for each of the 16 transmit channels. The chirp signal is generated by a high sampling rate DAC and this wide bandwidth signal is further upconverted to S-band using an image rejection mixer. This upconverted chirp signal acts as a carrier for modulating the multitone waveform on each transmitter. On the receive side, the S-band chirp signal is used for demodulating the received energy using an image rejection mixer and this signal is filtered and sampled by ADCs on the Nutaq devices. Two dedicated clock distribution modules (AD9510) are used to synchronize the RF Frontend with digital backend. The transmit antennas are placed with a spacing of $d_T = 0.5$ and the receive antenna elements are placed with a spacing of $d_R = 0.5N_T$ relative to the wavelength $\lambda_c = c/f_c$ of the carrier signal to obtain the virtual array with aperture length $N_T N_R$ meter where c is the velocity of light in vacuum, and f_c is the carrier frequency.

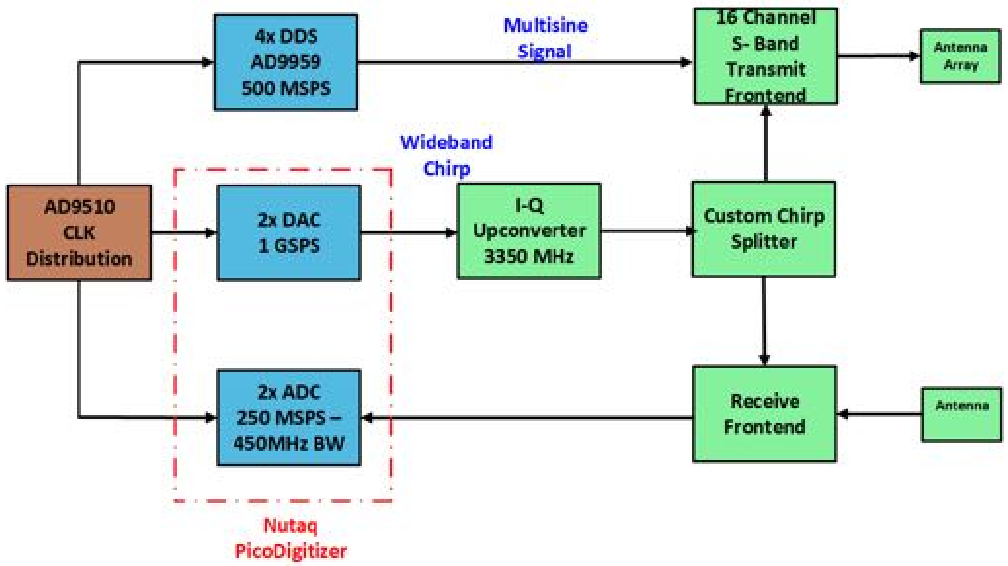

Figure 5: Block diagram of Compressive Radar system

The modulation and demodulation process is illustrated in Figure 6. The multitone signal is generated between 70 MHz - 230 MHz using DDS eval boards. The chirp signal of 30 MHz bandwidth is generated using the DAC present in Nutaq Picodigitizer. This chirp signal is upconverted to S-band (3350 MHz) using an image rejection mixer. This upconverted chip is filtered by a custom designed BPF to remove the side band and LO leaking from the mixer. The resulting upconverted chirp is fed to a custom designed chirp splitter board which further amplifies the signal and in turn splits the chirp signal to the 16 transmitter and two receivers. On transmit side, the multitone signal is modulated by the wideband chirp using a single sideband mixer. This modulated signal is further amplified by a power amplifier and filtered using a BPF to remove the side band arising from the mixer. On the receiver, the received energy is band pass filtered to minimize wideband thermal noise, and the filtered signal is downconverted using an image rejection mixer. This down converted signal is low pass filtered and sampled by the ADC for post processing. In order to get adequate frequency separation (140 MHz) between the fundamental and image component after upconversion, the starting frequency of the multitone signal was chosen to be 70 MHz. This eliminates the need for expensive band pass filters with aggressive roll off frequency. The upper limit of the multitone was chosen to be 230 MHz because, with a 500 Mega Samples per Second (MSPS) DAC, the digital image is at 270 MHz. This gives 40 MHz frequency separation for the low pass filter to attenuate the image component. High side injection is used on transmitter due to better Local Oscillator (LO) suppression by the BPF.

The main components of the compressive radar frontend are transmit frontend, receive frontend, RF chirp splitter board, and 16x1 antenna array. The entire RF Frontend, except the BPF, were designed using commercially available off the shelve components to save on cost, reduce the overall size, and make the system scalable for future needs. The RF traces were simulated and desinged as CPWG lines in Agilent ADS. To minimize the signal cross coupling and to reduce the power supply induced signal distortion, no two RF/IF components share the same bias network. The RF Frontend was fabricated on a four layer RO4350B substrate and designed using Cadence PCB Editor software.

The Nutaq Picodigitizer constitutes the digital backend for generating and sampling the radar waveform,

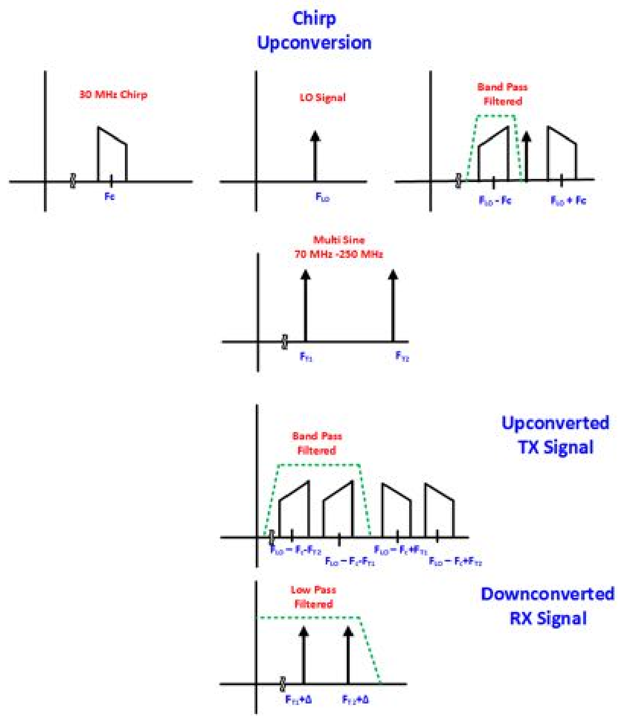

Figure 6: Spectrum of wideband chirp, multitone, transmit signal and receive signal. Passband frequency of filter shown as green dashed line.

and an embedded PC as a host to control the digital backend and to perform on the fly data processing. The digital processing hardware (ADAC250) is designed around the high-performance A/D and D/A conversion technology from Texas Instruments. It integrates one dual, 14-bit, 250 MSps ADC (ADS62P49) and a dual, 16-bit, 1 GSps DAC (DAC5682Z), also capable of operating in 2-4X interpolation mode. The max output power of the DAC at the operating frequency is 0 dBm and input saturation level of the ADC is 11 dBm. The analog bandwidth of the ADC is 450 MHz. The ADAC250 module is controlled by Virtex-6 Field Programmable Gate Array (FPGA) core which features 4GB DDR3 RAM and 64 GB solid state memory for real-time waveform scheduling.

Figure 7 shows the photo of the MIMO Compressive Radar test bed with its accessories mounted onto a cart. The transmit frontend, receive frontend, and the chirp splitter hardware are fabricated with surface mount components to save on cost and space. Analog Devices evaluation modules were used for the DDS, and clock distribution hardware. Agilent MXG N5183A signal generator is used for generating the 3205 MHz LO signal for up-converting the wideband chip and also provides the 10 MHz reference for the Nutaq Picodigitizer. The antenna array is connected to the transmit and receive frontend by a 1.8m 50 ohms flexible coaxial cable. A detailed description of the hardware design and characterization is discussed in [31].

2.4.2 Experimental results

The radar testbed was extensively characterized by closed-loop testing to verify the performance of the RF Frontend and the digital backend. After controlled environment testing, the multi-target experiments were

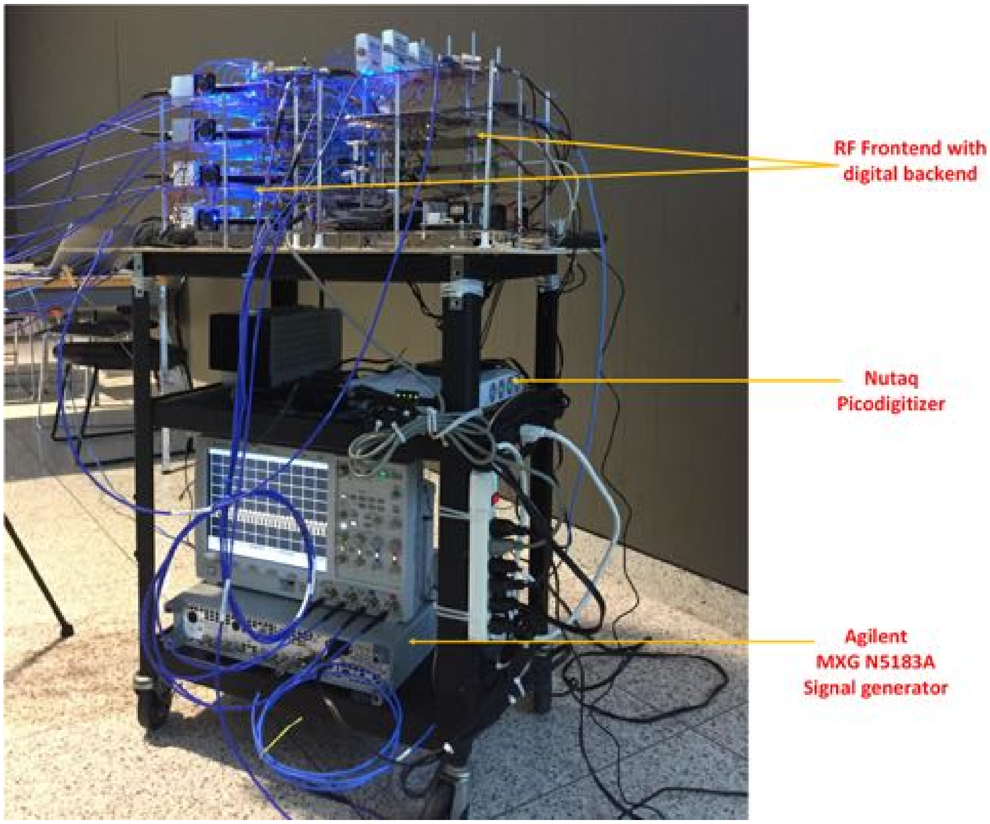

Figure 7: Radar testbed with accessories mounted on a cart

performed in an open parking space with a combination of trihedral and cylinders as radar targets. The sub-sampling factor ($\frac{t_u}{\tau}$) was kept as 0.041 for all the experiments. The phase calibration of the sixteen transmit channel was performed by placing a trihedral at 90° angle with respect to the antenna array. The results obtained from this experiment were used for calibrating the phase offset of the transmit array. Figure 8a shows the photo of the experimental setup with three targets (two trihedral and one cylinder) separated in range and angle. Figure 8b 8c shows the matched filter results with angle and range of three targets. Figure 8d shows the sub-sampled solver output of the trial.

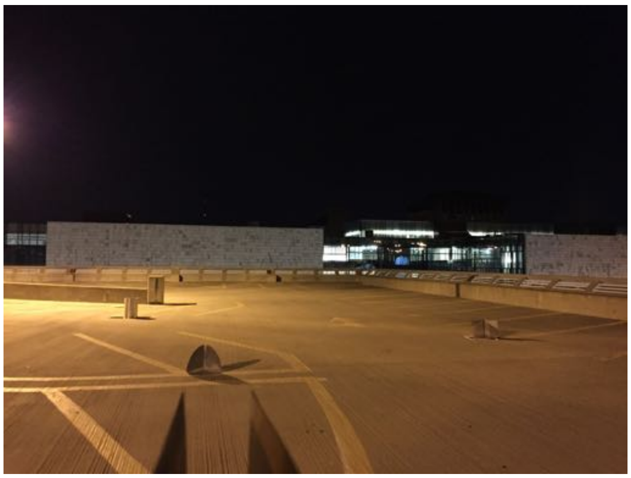

(a) Photo showing placement of three targets

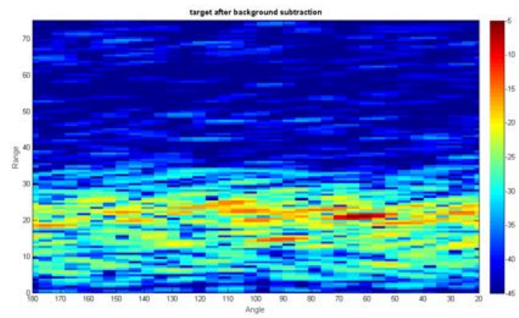

(b) Three target estimates after background subtraction

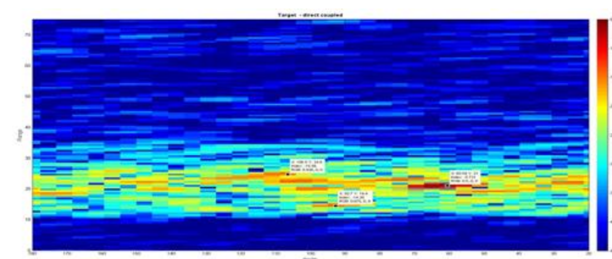

(c) Three target estimates after background subtraction and direct coupled removed

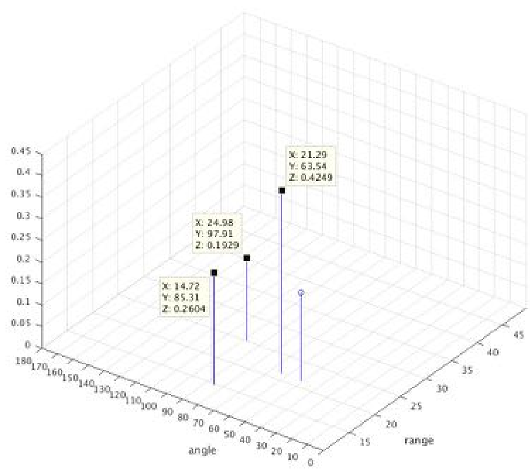

(d) Solver output for the three target

Figure 8: Three targets with two sets of frequency

References

[1] M. I. Skolnik, *Introduction to Radar Systems*, 3rd ed. ¡country¿US¡/country¿: McGraw-Hill Professional, 2002.

[2] R. H. Walden, "Analog-to-digital converter technology comparison," in *Proceedings of 1994 IEEE GaAs IC Symposium*, Oct 1994, pp. 217–219.

[3] M. A. Richards, *Fundamentals of Radar Signal Processing*. ¡country¿US¡/country¿: McGraw-Hill Professional, 2005.

[4] R. J. C. Middleton, "Dechirp-on-receive linearly frequency modulated radar as a matched-filter detector," *IEEE Transactions on Aerospace and Electronic Systems*, vol. 48, no. 3, pp. 2716–2718, JULY 2012.

[5] L. C. Potter, E. Ertin, J. T. Parker, and M. Cetin, "Sparsity and compressed sensing in radar imaging," *Proceedings of the IEEE*, vol. 98, no. 6, pp. 1006–1020, June 2010.

[6] K. Gedalyahu and Y. Eldar, "Time-delay estimation from low-rate samples: A union of subspaces approach," *IEEE Transactions on Signal Processing,*, vol. 58, no. 6, pp. 3017–3031, June 2010.

[7] C.-Y. Chen and P. Vaidyanathan, "Compressed sensing in mimo radar," in *Signals, Systems and Computers, 2008 42nd Asilomar Conference on*, Oct 2008, pp. 41–44.

[8] Y. Yu, A. Petropulu, and H. Poor, "Measurement matrix design for compressive sensing based mimo radar," *IEEE Transactions on Signal Processing*, vol. 59, no. 11, pp. 5338–5352, Nov. 2011.

[9] M. Herman and T. Strohmer, "High-resolution radar via compressed sensing," *IEEE Transactions on Signal Processing*, vol. 57, no. 6, pp. 2275–2284, June 2009.

[10] T. Strohmer and B. Friedlander, "Analysis of sparse mimo radar," *Applied and Computational Harmonic Analysis*, vol. 37, no. 3, pp. 361 – 388, 2014.

[11] T. Strohmer and H. Wang, "Accurate imaging of moving targets via random sensor arrays and kerdock codes," *Inverse Problems*, vol. 29, no. 8, p. 085001, 2013.

[12] D. Dorsch and H. Rauhut, "Refined analysis of sparse MIMO radar," *CoRR*, vol. abs/1509.03625, 2015.

[13] M. Hgel, H. Rauhut, and T. Strohmer, "Remote sensing via ℓ_1-minimization," *Foundations of Computational Mathematics*, vol. 14, no. 1, pp. 115–150, 2014.

[14] Y. Yu, A. Petropulu, and H. Poor, "Cssf mimo radar: Compressive-sensing and step-frequency based mimo radar," *IEEE Transactions on Aerospace and Electronic Systems*, vol. 48, no. 2, pp. 1490–1504, APRIL 2012.

[15] B. Li and A. Petropulu, "Rip analysis of the measurement matrix for compressive sensing-based mimo radars," in *IEEE 8th Sensor Array and Multichannel Signal Processing Workshop (SAM), 2014*, June 2014, pp. 497–500.

[16] Z. Slavik, A. Viehl, T. Greiner, O. Bringmann, and W. Rosenstiel, "Compressive sensing-based noise radar for automotive applications," in *2016 12th IEEE International Symposium on Electronics and Telecommunications (ISETC)*, Oct 2016, pp. 17–20.

[17] T. Ragheb, J. N. Laska, H. Nejati, S. Kirolos, R. G. Baraniuk, and Y. Massoud, "A prototype hardware for random demodulation based compressive analog-to-digital conversion," in *2008 51st Midwest Symposium on Circuits and Systems*, Aug 2008, pp. 37–40.

[18] S. Kirolos, T. Ragheb, J. Laska, M. F. Duarte, Y. Massoud, and R. G. Baraniuk, "Practical issues in implementing analog-to-information converters," in *2006 6th International Workshop on System on Chip for Real Time Applications*, Dec 2006, pp. 141–146.

[19] J. Yoo, S. Becker, M. Loh, M. Monge, E. Cands, and A. Emami-Neyestanak, "A 100mhz−2ghz 12.5x sub-nyquist rate receiver in 90nm cmos," in *2012 IEEE Radio Frequency Integrated Circuits Symposium*, June 2012, pp. 31–34.

[20] M. Wakin, S. Becker, E. Nakamura, M. Grant, E. Sovero, D. Ching, J. Yoo, J. Romberg, A. Emami-Neyestanak, and E. Candes, "A nonuniform sampler for wideband spectrally-sparse environments," *IEEE Journal on Emerging and Selected Topics in Circuits and Systems*, vol. 2, no. 3, pp. 516–529, Sep. 2012.

[21] M. Mishali, Y. C. Eldar, O. Dounaevsky, and E. Shoshan, "Xampling: Analog to digital at sub-nyquist rates," *IET Circuits, Devices Systems*, vol. 5, no. 1, pp. 8–20, January 2011.

[22] M. Mishali, R. Hilgendorf, E. Shoshan, I. Rivkin, and Y. C. Eldar, "Generic sensing hardware and real-time reconstruction for structured analog signals," in *2011 IEEE International Symposium of Circuits and Systems (ISCAS)*, May 2011, pp. 1748–1751.

[23] M. Mishali and Y. C. Eldar, "From theory to practice: Sub-nyquist sampling of sparse wideband analog signals," *IEEE Journal of Selected Topics in Signal Processing*, vol. 4, no. 2, pp. 375–391, April 2010.

[24] D. J. K. Adams, "A practical implementation of the modulated wideband converter compressive sensing receiver architecture," Ph.D. dissertation, Stanford University, 2016.

[25] M. Mishali, Y. C. Eldar, and A. J. Elron, "Xampling: Signal acquisition and processing in union of subspaces," *IEEE Transactions on Signal Processing*, vol. 59, no. 10, pp. 4719–4734, Oct 2011.

[26] E. Baransky, G. Itzhak, N. Wagner, I. Shmuel, E. Shoshan, and Y. Eldar, "Sub-nyquist radar prototype: Hardware and algorithm," *IEEE Transactions on Aerospace and Electronic Systems*, vol. 50, no. 2, pp. 809–822, April 2014.

[27] D. Cohen, D. Cohen, Y. C. Eldar, and A. M. Haimovich, "Sub-nyquist collocated mimo radar in time and space," in *2016 IEEE Radar Conference (RadarConf)*, May 2016, pp. 1–4.

[28] D. Cohen, A. Dikopoltsev, R. Ifraimov, and Y. C. Eldar, "Towards sub-nyquist cognitive radar," in *2016 IEEE Radar Conference (RadarConf)*, May 2016, pp. 1–4.

[29] E. Ertin, "Frequency diverse waveforms for compressive radar sensing," in *2010 International Waveform Diversity and Design Conference*, Aug 2010, pp. 000 216–000 219.

[30] E. Ertin, L. C. Potter, and R. L. Moses, "Sparse target recovery performance of multi-frequency chirp waveforms," in *2011 19th European Signal Processing Conference*, Aug 2011, pp. 446–450.

[31] S. Baskar, "Tranmsitter architecture for multi input multi output compressive radar," Ph.D. dissertation, The Ohio State University, 2017.

NATO OTAN SCIENCE AND TECHNOLOGY ORGANIZATION COLLABORATION SUPPORT OFFICE

Lecture Series Notes on Compressive Sensing Techniques for Radar and ESM Applications:

Part I: Application of Compressive Sensing to 2D/3D SAR
Part II: Hardware Architectures for Compressive Sensing

Emre Ertin
The Ohio State University
2/4/19

RLS SET-257 Date - Location 1

NATO OTAN SCIENCE AND TECHNOLOGY ORGANIZATION COLLABORATION SUPPORT OFFICE

Part I: Application of Compressive Sensing to 2D/3D SAR

RLS SET-257 Date - Location 2

SCIENCE AND TECHNOLOGY ORGANIZATION
COLLABORATION SUPPORT OFFICE

Circular SAR

Circular SAR provides information about the 3D location of the scattering centers and their reflectivity as a function of aspect angle

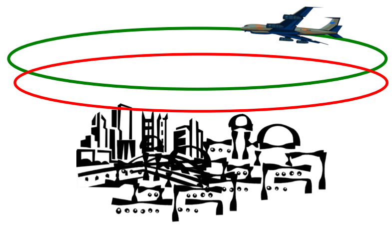

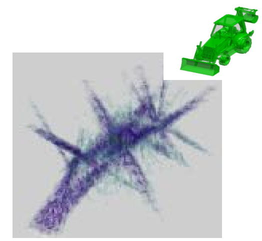

- 3D Resolution of Circular SAR is constrained by
  - Limited Persistence of Reflectors
  - Sparse Elevation Sampling
  - Dynamically varying nonuniform spacing in elevation

SCIENCE AND TECHNOLOGY ORGANIZATION
COLLABORATION SUPPORT OFFICE

Outline

- Circular SAR Processing for 3D image products
  - Review of Fourier Imaging
  - Post processing for 3D information
- Characterization of 3D resolution as a function of
  - Persistence, Bandwidth, Location
- Enhanced Imaging for 2D and 3D
  - Deconvolution of point spread function
  - Regularization through sparsity constraints

NATO OTAN SCIENCE AND TECHNOLOGY ORGANIZATION COLLABORATION SUPPORT OFFICE

Fourier Theory

- Ground plane imagery is obtained by projecting conical grid in (k_x, k_y, k_z) to (k_x, k_y) plane and IFT

$$
\begin{aligned}
k_x &= \frac{4\pi f}{c}\cos(az)\cos(el)\\
k_y &= \frac{4\pi f}{c}\sin(az)\cos(el)\\
k_z &= \frac{4\pi f}{c}\sin(el)
\end{aligned}
$$

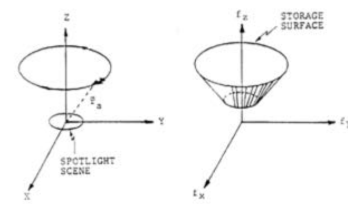

[Brown, 1980]

NATO OTAN SCIENCE AND TECHNOLOGY ORGANIZATION COLLABORATION SUPPORT OFFICE

2D Image Reconstruction

- Enhanced Imaging use sparsity constrained optimization techniques [Cetin, 2004] to find a sparse description of the scene that is consistent with the phase history data (Deconvolution of the PSF)

$$\arg\min_x\{\|H * x - y\|^2 + \lambda\|x\|^p\}$$

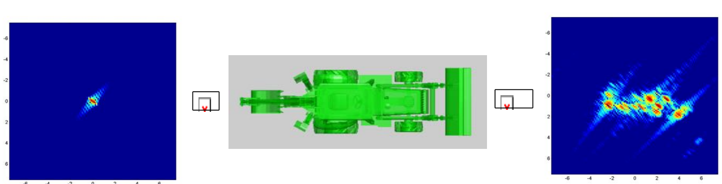

SPIE 2007 6

SCIENCE AND TECHNOLOGY ORGANIZATION
COLLABORATION SUPPORT OFFICE

2D Image Enhancement

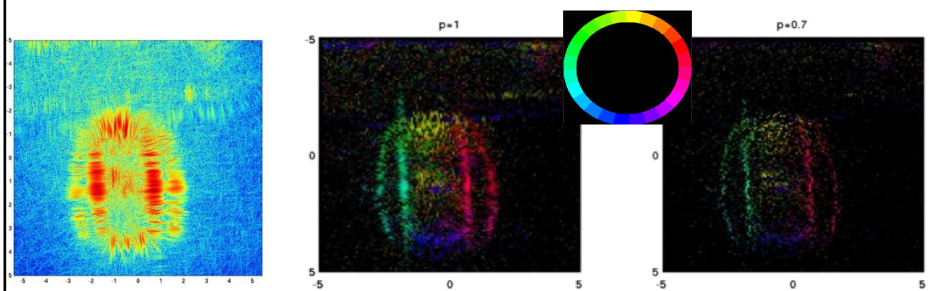

Circular aperture reveals scattering behavior as a function of aspect angle

SPIE 2007 7

SCIENCE AND TECHNOLOGY ORGANIZATION
COLLABORATION SUPPORT OFFICE

Multipass Interferometric SAR

$$I_i(x_l, y_l) = \sum_p \tilde{g}_p(x_l, y_l) e^{-jh_p(x_l,y_l)k_p i}$$

- Detection: Eigenvalues of the sample covariance matrix for detecting the number of scattering centers

  Estimation: ESPRIT spectral estimation method for estimating their heights

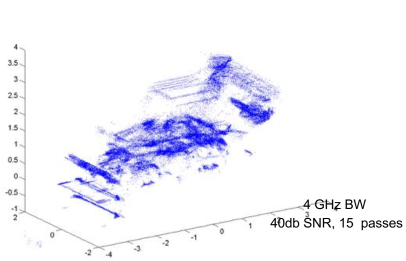

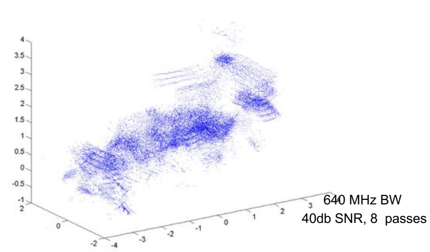

NATO OTAN SCIENCE AND TECHNOLOGY ORGANIZATION COLLABORATION SUPPORT OFFICE

Resolution for Circular SAR

- 3D resolution requires both reflector persistence and a wide-aperture.
- IPR nulls are insufficient to characterize 3D resolution.

NATO OTAN SCIENCE AND TECHNOLOGY ORGANIZATION COLLABORATION SUPPORT OFFICE

3D Direct Fourier Imaging

- 3D Volume by stacking 2D images

$$I(x, y, z) = \sum_{z} f_z(x, y)\delta(z - z_0)$$

– Image for the plane $f(x, y)\delta(z - z_0)$ can be obtained by applying a phas to each point in the conical grid

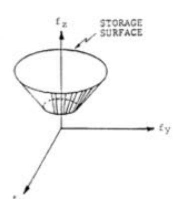

$$I(k_x, k_y, k_z)\exp(-jk_z z_0)$$

SCIENCE AND TECHNOLOGY ORGANIZATION
COLLABORATION SUPPORT OFFICE

Multipass Interferometric SAR

- Employ high resolution parametric spectral estimation methods to mitigate the effects of sparse elevation sampling
[Xiao and Munson 1998, Gini and Lombardini 2005]
- Relative phase of the 2D images formed from different passes provide height information for the scattering centers in each resolution cell

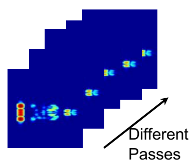

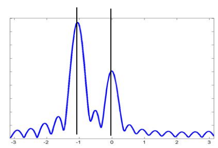

$$I_i(x_l, y_l) = \sum_p \tilde{g}_p(x_l, y_l) e^{-jh_p(x_l,y_l)k_p i}$$

◆ **Sum of complex exponentials model**

SCIENCE AND TECHNOLOGY ORGANIZATION
COLLABORATION SUPPORT OFFICE

Multipass Interferometric SAR

$$I_i(x_l, y_l) = \sum_p \tilde{g}_p(x_l, y_l) e^{-jh_p(x_l,y_l)k_p i}$$

- Detection: Eigenvalues of the sample covariance matrix for detecting the number of scattering centers

  Estimation: ESPRIT spectral estimation method for estimating their heights

Model Order	1	2	3
Percentage of Resolution Cells	71.88	27.11	1.01

NATO OTAN
SCIENCE AND TECHNOLOGY ORGANIZATION
COLLABORATION SUPPORT OFFICE
S&T organization CSO

Nonuniform Elevation Sampling

- Real world flight paths
  - Unequispaced elevation cuts

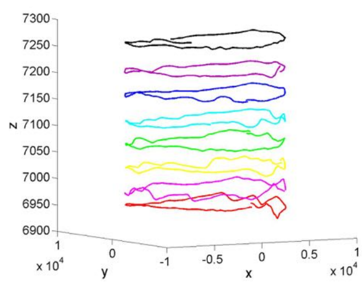

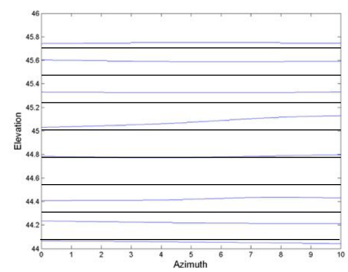

NATO OTAN
SCIENCE AND TECHNOLOGY ORGANIZATION
COLLABORATION SUPPORT OFFICE
S&T organization CSO

Nonuniform Elevation Sampling

- Start with Linear Interpolation

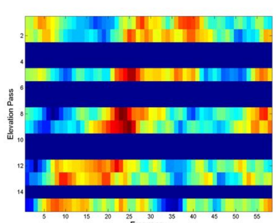

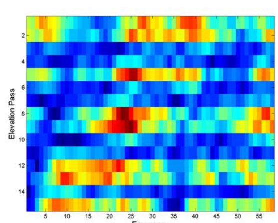

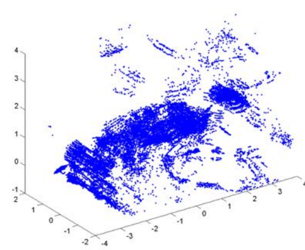

SCIENCE AND TECHNOLOGY ORGANIZATION
COLLABORATION SUPPORT OFFICE

Interpolation through enhancement of single pulse images

- For each pulse from the eight passes we can form a 2D range-height image. Due to sparse sampling in elevation the resulting images have poor resolution (large sidelobes) in height
- Enhancement of these images will result in effect interpolation of phase history in elevation

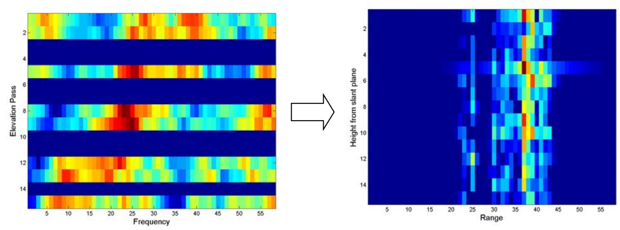

SCIENCE AND TECHNOLOGY ORGANIZATION
COLLABORATION SUPPORT OFFICE

Deconvolution of point spread funtion

Deconvolution of point spread function is an ill posed problem. We employ a sparsity regularized reconstruction approach to single pulse images [Cetin, 2004]

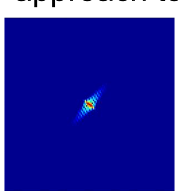

H

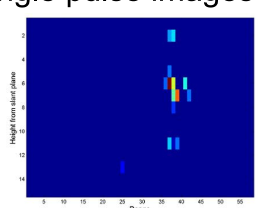

x

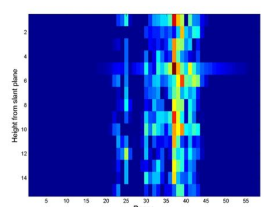

y

$$\arg\min_{x}\{\underbrace{\|H * x - y\|^2}_{\text{Likelihood: physical model and sparse representation}} + \underbrace{\lambda\|x\|^p}_{\text{Prior (regularization)}}\}$$

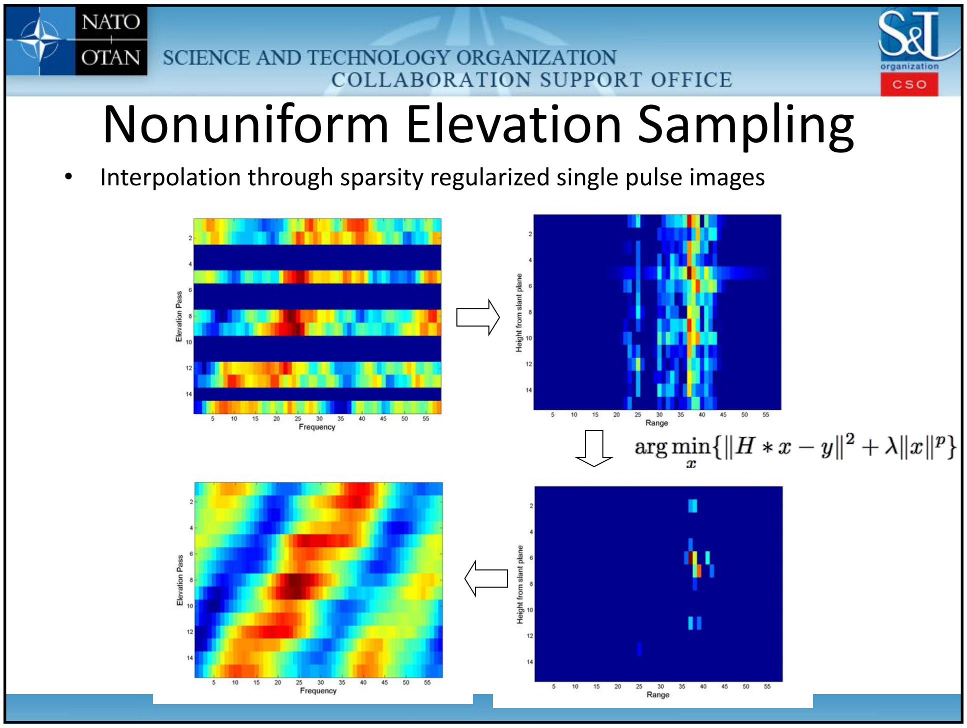
NATO
OTAN
SCIENCE AND TECHNOLOGY ORGANIZATION
COLLABORATION SUPPORT OFFICE
S&T organization
CSO
Nonuniform Elevation Sampling
• Interpolation through sparsity regularized single pulse images
Elevation Pass
Frequency
Height from slant plane
Range
$\arg\min_{x}\{\|H * x - y\|^2 + \lambda\|x\|^p\}$
Elevation Pass
Frequency
Height from slant plane
Range

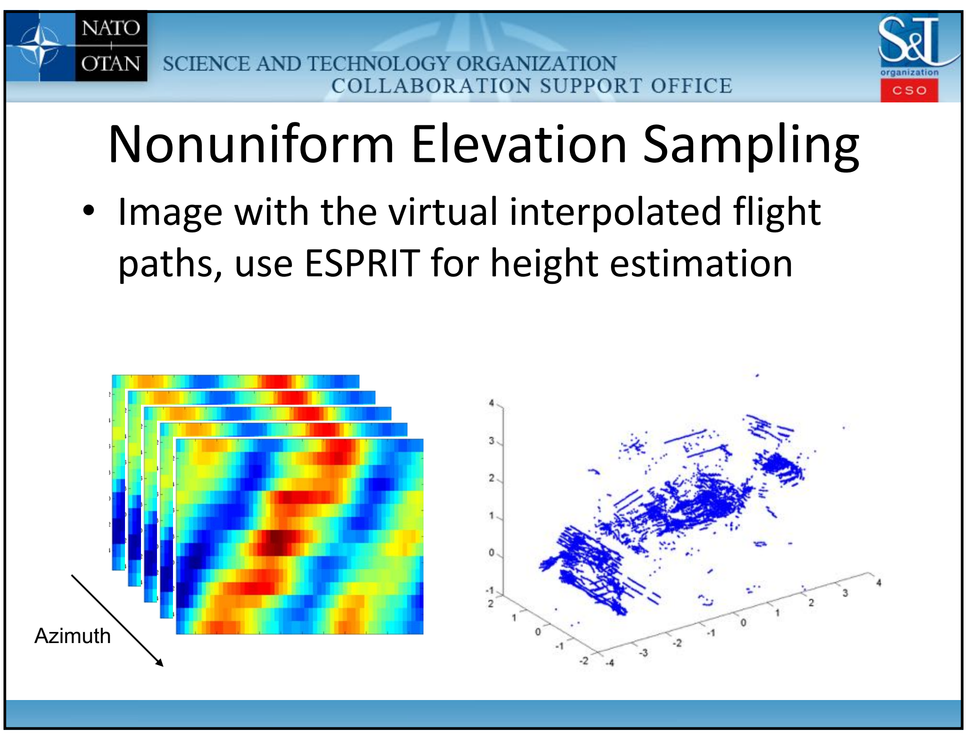
NATO
OTAN
SCIENCE AND TECHNOLOGY ORGANIZATION
COLLABORATION SUPPORT OFFICE
S&T organization
CSO
Nonuniform Elevation Sampling
• Image with the virtual interpolated flight paths, use ESPRIT for height estimation
Azimuth

SCIENCE AND TECHNOLOGY ORGANIZATION
COLLABORATION SUPPORT OFFICE

l_p Regularized Least-Squares (LS)

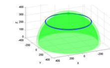

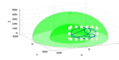

- Sparsity
  - Measurements y : sparse sampling of full (f,az,el) radar measurement space.
  - Reconstruction: x sparse set of (x,y,z) locations with significant radar scattering energy.
- Linear Model

$$y = Ax + \nu$$

$$A = \left[e^{-j(k_{x,m}x_n + k_{y,m}y_n + k_{z,m}z_n)} \right], \quad M \times V$$

$$\hat{x} = \arg\min_x \; \|y - Ax\|_2^2 + \lambda \|x\|_p^p \quad p \le 1$$

SCIENCE AND TECHNOLOGY ORGANIZATION
COLLABORATION SUPPORT OFFICE

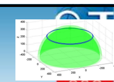

l_p Regularized LS

Top 40 dB; p=1; λ=10; 5° subapertures, HH, VV

Multi-pass IFSAR

Top 20 dB; p=1; 5° subapertures; HH, VV

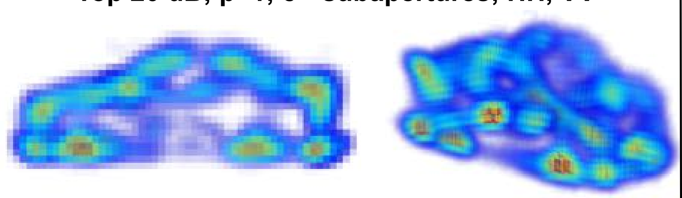

Fourier

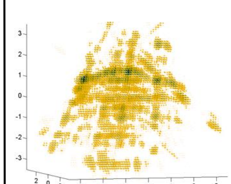

Top 20 dB

NATO OTAN
SCIENCE AND TECHNOLOGY ORGANIZATION
COLLABORATION SUPPORT OFFICE

- Algorithm variables
  - N: Number of samples in x,y,z dimensions
  - K: Number of IFSAR passes.
  - κ=cond(A^HA+D(i))

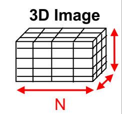

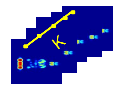

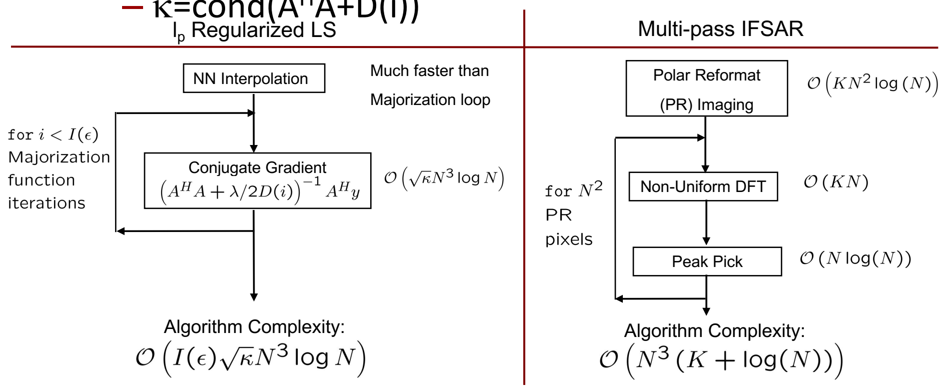

NATO OTAN
SCIENCE AND TECHNOLOGY ORGANIZATION
COLLABORATION SUPPORT OFFICE

Part II: Hardware Architectures for Compressive Sensing

RLS SET-257 Date - Location 22

SCIENCE AND TECHNOLOGY ORGANIZATION
COLLABORATION SUPPORT OFFICE

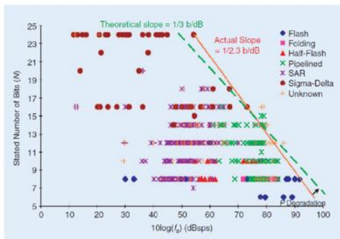

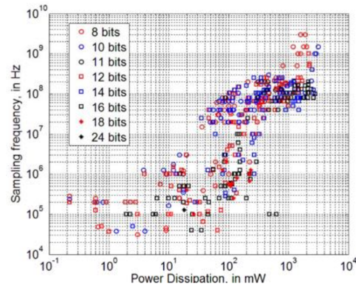

- Resolution of ADC decreases with increase in sampling rate [1]
- Power consumption quadruples for additional bit of resolution [1]
- High sampling rate with increase in RX channels generates huge amount of data for storage and processing

SCIENCE AND TECHNOLOGY ORGANIZATION
COLLABORATION SUPPORT OFFICE

Overview

- Requirements for High Resolution Radar Systems
- Receiver Side CS Architectures
- Compressive Illumination Radar Sensor Implementation
- Experiment results

NATO OTAN SCIENCE AND TECHNOLOGY ORGANIZATION COLLABORATION SUPPORT OFFICE

Compressive sampling ADC (CADC)

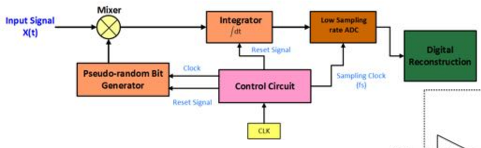

Random Modulator based CADC [2]

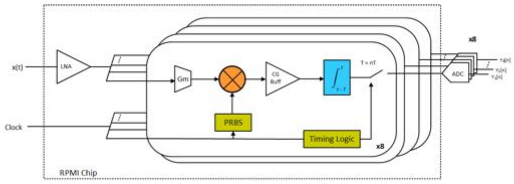

Random Modulator Pre-Integrator architecture [5]

- Input signal is spread over wider band, low pass filtered and sampled at lower rate [2, 3]
- PRBS needs to be generated at Nyquist rate of input system- Practical constraint [4]
- Requires redesigning the ADC, not readily available
- Practical implementation- 8 channel CMOS receiver – analog bandwidth of 100 MHz -2 GHz with dynamic range of 54 dB [5]

NATO OTAN SCIENCE AND TECHNOLOGY ORGANIZATION COLLABORATION SUPPORT OFFICE

Non-Uniform Sampler (NUS) for Wideband Spectrally-Sparse Signals

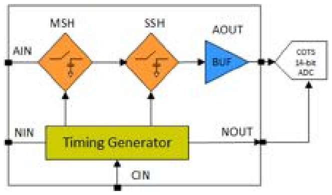

Block diagram of NUS receiver for spectrally-sparse signals [6]

- Timing Generator generates non-uniformly spaced pulse train for controlling master and slave sample-and-hold circuits which sample segments of sparse i/p signal.
- Samples are buffered amplified and digitized by a non-uniform sampling ADC at a sampling rate much lower than the Nyquist.
- Even though this architecture is simple to implement compared to CADC, input signal bound by two main constraints
    - Effective Instantaneous Bandwidth (EIBW) of I/P signal should be less than half Nyquist rate
    - I/P signal should be spectrally sparse in order to achieve accurate reconstruction

SCIENCE AND TECHNOLOGY ORGANIZATION
COLLABORATION SUPPORT OFFICE

Modulated wideband converter

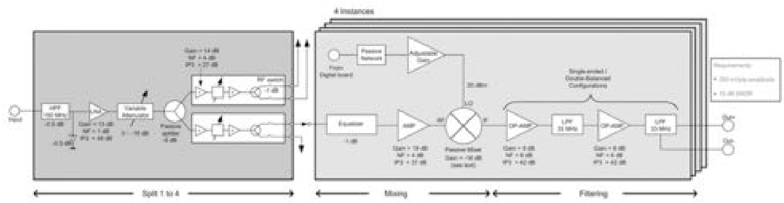

Block diagram of MWC analog board [7]

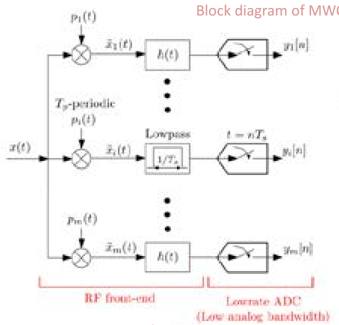

MWC architecture

- Instead of PRBS, transient periodic waveforms generated by Shift registers used
- Can be implemented with simple switching mixer and equalizer
- Architecture bounded by fs = $\frac{Nyquist}{M}$
- Reduction in sampling rate is linearly proportional to number of channels
- Lower sampling rate is possible with more RX channels

SCIENCE AND TECHNOLOGY ORGANIZATION
COLLABORATION SUPPORT OFFICE

Compressive receiver

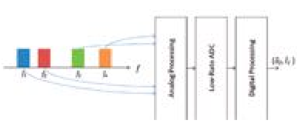

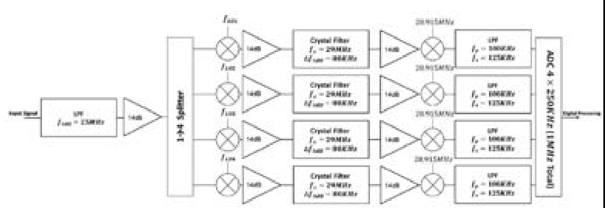

4 Channel crystal receiver with proposed sampling scheme [8]

- Sub-Nyquist radar prototype based on Xampling framework – 87.5% compression rate [15]
- Requires 3 filtering stages which adds to cost and complexity of design
- Requires 2 mixing stages which suffer from problems like inter modulation and LO leakage which affects the dynamic range of the system.

Novel Compressive Radar architecture

- Radar sensing is not just receive processing:

  Illumination+ Receiver Filtering+ Sampling

- Compressive Illumination scheme- Transmit waveform with randomness + compressive sampling at stretch process receiver
- Requirement: uniform sampling ADC with high analog bandwidth

  analog BW > sampling rate

Conventional Digital SDR Arhitecture

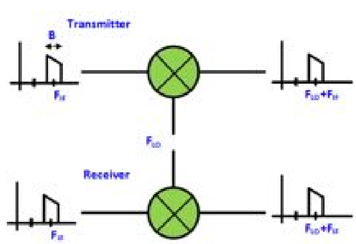

- Range = delay in received signal
- Sampling rate = 2xB
- B =2 GHz , sampling rate = 4 GSps

SCIENCE AND TECHNOLOGY ORGANIZATION
COLLABORATION SUPPORT OFFICE

Stretch Processing receivers

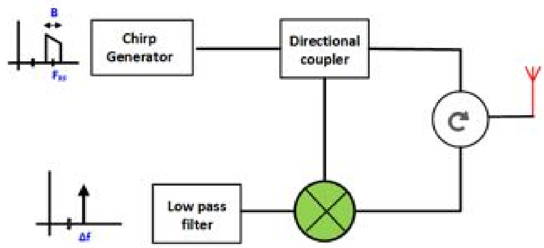

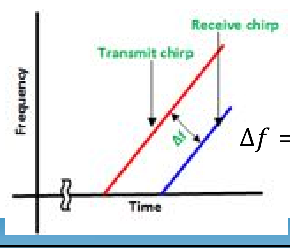

$\Delta f = \frac{B}{\tau} t_d$

- Range = change in frequency on receive
- B =2 GHz , t_u = 1000 m, τ =80 µs

  Δf = 166.5 MHz
- Sampling rate = $2x\Delta f$ = 333 MSps

SCIENCE AND TECHNOLOGY ORGANIZATION
COLLABORATION SUPPORT OFFICE

Compressive Illumination

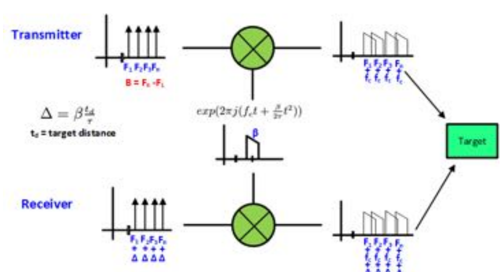

New Sampling rate = $\frac{\beta}{\tau} t_u$ instead of $\frac{B}{\tau} t_u$

where β = bandwidth of chirp, t_u = unambiguous time, τ = pulse duration

β = 30 MHz , T_u = 1000 m, τ =80 µs Δf = 1.998 MHz

System Bandwidth (B) = $(F_1 - F_N)$

NATO OTAN SCIENCE AND TECHNOLOGY ORGANIZATION COLLABORATION SUPPORT OFFICE

Proposed CS Radar - MIMO

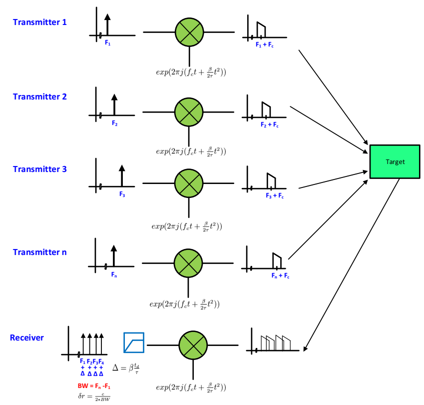

- Extending concept to MIMO for detecting Distance and Direction
- 1 tone per TX channel – no issues with linearity and PAPR with PA

NATO OTAN SCIENCE AND TECHNOLOGY ORGANIZATION COLLABORATION SUPPORT OFFICE

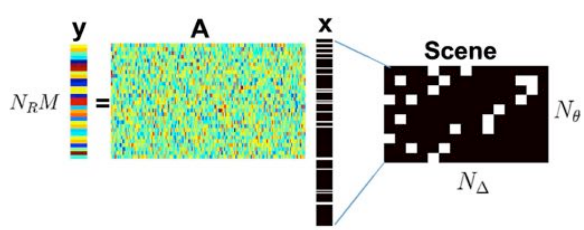

$$min \parallel x \parallel_1 \text{ Subject to } \parallel Ax - y \parallel_2 \leq \sigma^2$$

We present two solutions

1. Match Filter $\hat{X}_{MF} = A^H y$
2. Sparsity regularization
   - Range space is discretized with resolution $\Delta_R = \frac{c}{2B}$
   - The non-linear mapping cos(θ) of the angle of arrival is discretized with resolution $\Delta_\theta = \frac{1}{N_T N_R}$

NATO OTAN SCIENCE AND TECHNOLOGY ORGANIZATION COLLABORATION SUPPORT OFFICE S&T organization CSO

- Requirements for High Resolution Radar Systems
- Receiver Side CS Architectures
- Compressive Illumination Radar Sensor Implementation
- Experiment results

NATO OTAN SCIENCE AND TECHNOLOGY ORGANIZATION COLLABORATION SUPPORT OFFICE S&T organization CSO

Compressive Radar System Overview

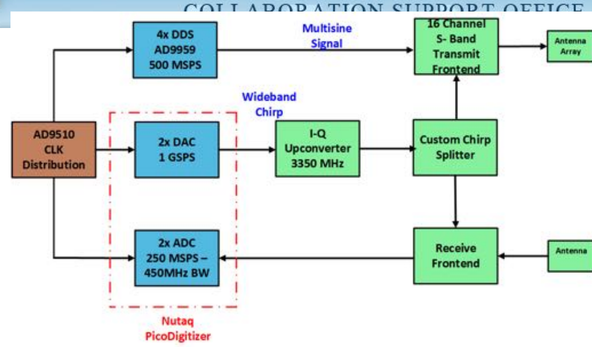

- DDS instead of DAC – low cost can be scaled in volume
- 16 Transmit channels – Single I/Q receive channel
- Custom chirp splitter board sourcing LO to 32 TX and 2 RX channels
- Nutaq Digital backend with 250 MSPS ADCs with 450 MHz analog BW
- Custom phase and delay synchronization architecture

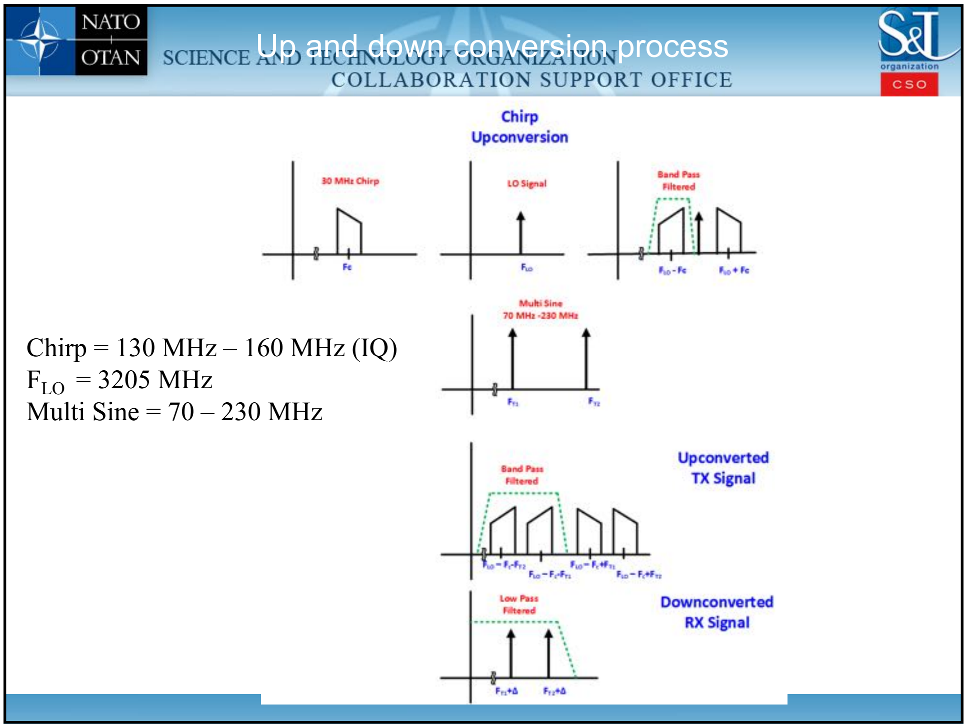
NATO
OTAN
SCIENCE AND TECHNOLOGY ORGANIZATION
COLLABORATION SUPPORT OFFICE
Up and down conversion process
Chirp
Upconversion
30 MHz Chirp
Fc
LO Signal
F_{LO}
Band Pass
Filtered
F_{LO} - Fc
F_{LO} + Fc
Chirp = 130 MHz – 160 MHz (IQ)
F_{LO} = 3205 MHz
Multi Sine = 70 – 230 MHz
Multi Sine
70 MHz -230 MHz
F_{T1}
F_{T2}
Upconverted
TX Signal
Band Pass
Filtered
Low Pass
Filtered
Downconverted
RX Signal
$F_{T1}+\Delta$
$F_{T2}+\Delta$

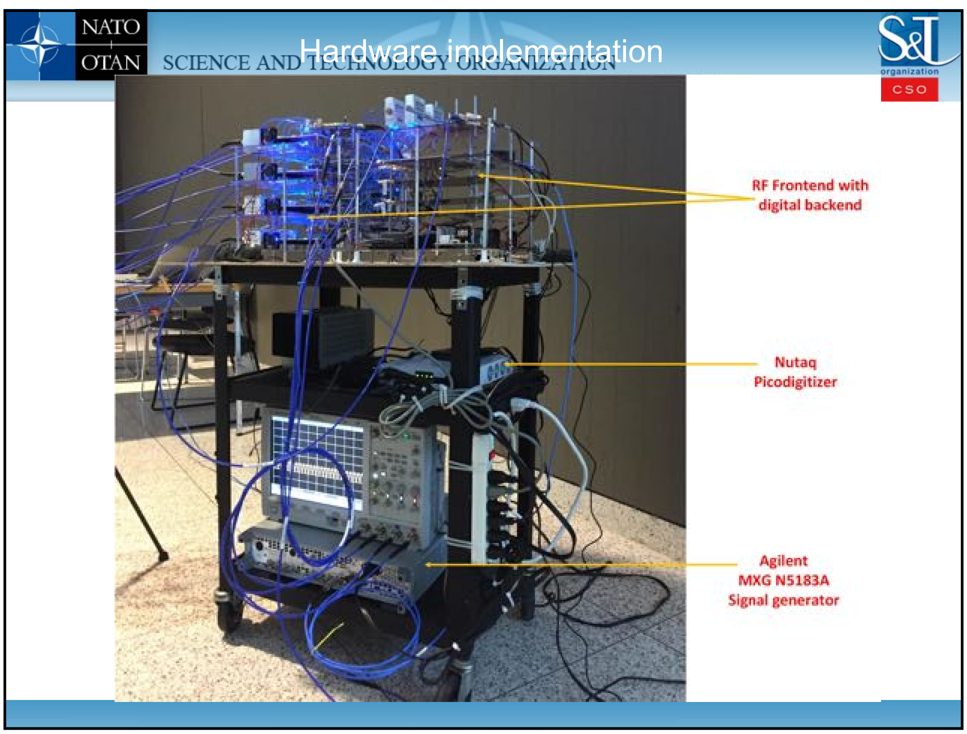
NATO
OTAN
SCIENCE AND TECHNOLOGY ORGANIZATION
Hardware implementation
RF Frontend with
digital backend
Nutaq
Picodigitizer
Agilent
MXG N5183A
Signal generator

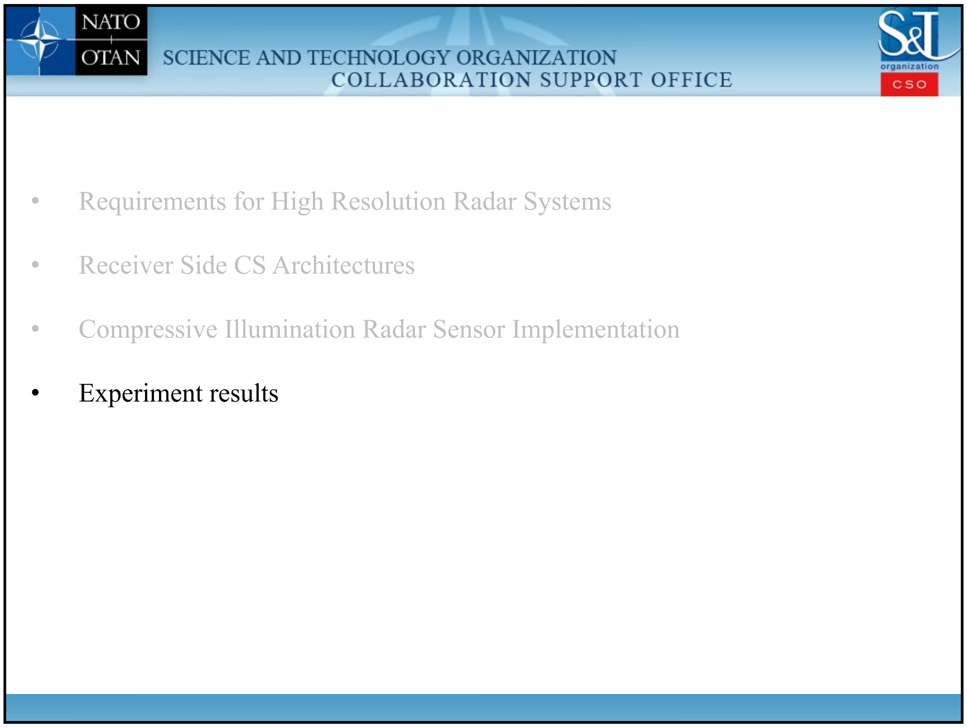
NATO
OTAN
SCIENCE AND TECHNOLOGY ORGANIZATION
COLLABORATION SUPPORT OFFICE
S&T organization
CSO
• Requirements for High Resolution Radar Systems
• Receiver Side CS Architectures
• Compressive Illumination Radar Sensor Implementation
• Experiment results

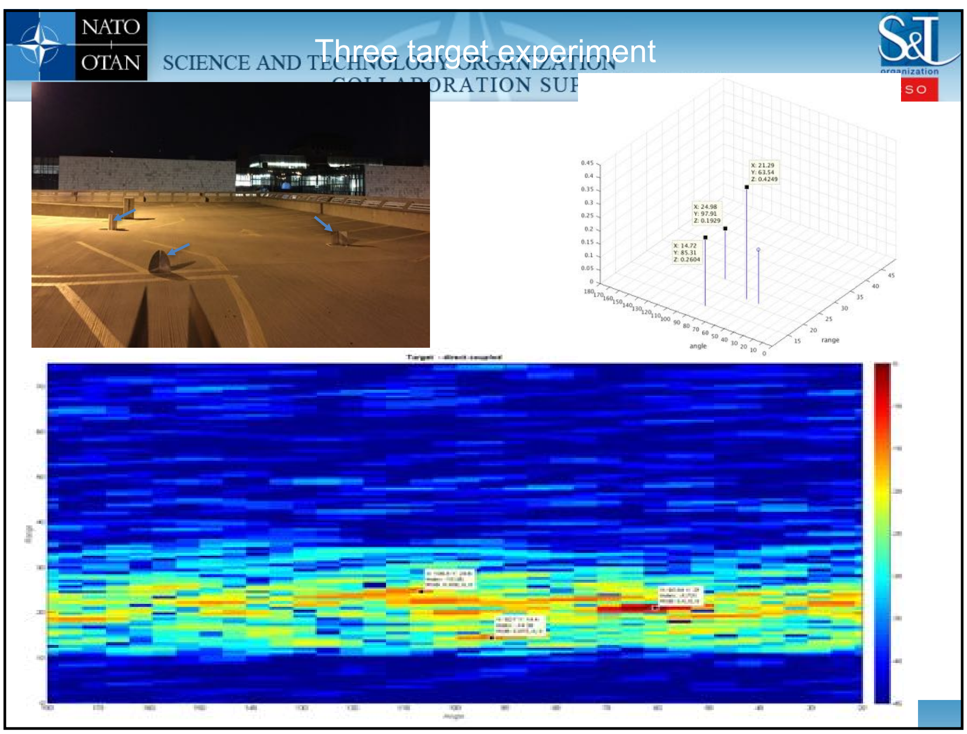
Three target experiment
X: 21.29
Y: 63.54
Z: 0.4249
X: 24.98
Y: 97.91
Z: 0.1929
X: 14.72
Y: 85.31
Z: 0.2604
angle
range

NATO OTAN SCIENCE AND TECHNOLOGY ORGANIZATION COLLABORATION SUPPORT OFFICE

References

1. R. H. Walden, "Analog-to-digital converter technology comparison," in Gallium Arsenide Integrated Circuit (GaAs IC) Symposium, 1994. Technical Digest 1994., 16th Annual, Oct 1994, pp. 217{219}.
2. T. Ragheb, J. N. Laska, H. Nejati, S. Kirolos, R. G. Baraniuk, and Y. Massoud, "A prototype hardware for random demodulation based compressive analog-to-digital conversion," in 2008 51st Midwest Symposium on Circuits and Systems, Aug 2008, pp. 37- 40.
3. J. Laska, S. Kirolos, Y. Massoud, R. Baraniuk, A. Gilbert, M. Iwen, and M. Strauss, "Random sampling for analog-to-information conversion of wideband signals," in 2006 IEEE Dallas/CAS Workshop on Design, Applications, Integration and Software, Oct 2006, pp. 119-122.
4. S. Kirolos, T. Ragheb, J. Laska, M. F. Duarte, Y. Massoud, and R. G. Baraniuk, "Practical issues in implementing analog-to-information converters," in 2006 6th International Workshop on System on Chip for Real Time Applications, Dec 2006, pp. 141-146.
5. J. Yoo, S. Becker, M. Loh, M. Monge, E. Cands, and A. Emami-Neyestanak, "A 100mhz x2013;2ghz 12.5x sub-nyquist rate receiver in 90nm cmos," in 2012 IEEE Radio Frequency Integrated Circuits Symposium, June 2012, pp. 31-34
6. M. Wakin, S. Becker, E. Nakamura, M. Grant, E. Sovero, D. Ching, J. Yoo, J. Romberg, A. Emami- Neyestanak, and E. Candes, "A nonuniform sampler for wideband spectrally-sparse environments, IEEE Journal on Emerging and Selected Topics in Circuits and Systems, vol. 2, no. 3, pp. 516–529, Sep. 2012.
7. M. Mishali, Y. C. Eldar, O. Dounaevsky, and E. Shoshan. Xampling: Analog to digital at sub-nyquist rates. IET Circuits, Devices Systems, 5(1):8{20, January 2011.
8. E. Baransky, G. Itzhak, N. Wagner, I. Shmuel, E. Shoshan, and Y. Eldar, "Sub-nyquist radar prototype: Hardware and algorithm," IEEE Transactions on Aerospace and Electronic Systems,, vol. 50, no. 2, pp. 809-822, Apr. 2014.